Block Copolymer Vesicles in Liquid CO_2

William F. Edmonds,[†] Marc A. Hillmyer,*[,‡] and Timothy P. Lodge*[,†,‡]

Department of Chemical Engineering and Materials Science and Department of Chemistry, University of Minnesota, Minneapolis, Minnesota 55455

Received February 18, 2007; Revised Manuscript Received May 7, 2007

ABSTRACT: Two polylactide-*b*-poly(perfluoropropylene oxide) (PLA−PFPO) diblock copolymers were synthesized via a coupling reaction of acid chloride end-functionalized poly(perfluoropropylene oxide) and hydroxy-terminated polylactide. The solubility of these materials in CO_2 was measured using a variable-volume high-pressure cell. At a concentration of 1 wt %, the PLA−PFPO copolymers were found to be soluble at modest pressures (<500 bar) over the temperature range of 30−65 °C. The size of the resulting micelles in solution was characterized by high-pressure dynamic light scattering. These measurements indicated the formation of predominantly small, spherical micelles for the block copolymer with a PFPO volume fraction of 0.49 and large aggregates with hydrodynamic radii of 100 nm for PLA−PFPO with a PFPO volume fraction of 0.37. By kinetically trapping the aggregates in CO_2 through vitrification of the PLA cores, redispersing them in an analogous PFPO selective solvent, and imaging them using transmission electron microscopy, we confirmed the formation of block copolymer vesicles in liquid CO_2.

Introduction

Diblock copolymers dissolved in a selective solvent self-assemble to form micelles. Spherical, cylindrical, and bilayer aggregates have been observed in several systems; accessing this progression of micelle structures is achieved experimentally by either increasing the core block length,[1] decreasing the corona block length,[2,3] or increasing the solvent selectivity.[3−8] These tunable variables afford specific control over micelle structure, which is imperative for tailoring solutions to specialized applications.[9] To date, this morphological progression has not been extended to compressible solvents, such as carbon dioxide, thereby limiting their potential as solvent alternatives.

The interest in condensed CO_2 is driven by its modest critical parameters (T_c = 31.1 °C, P_c = 73.8 bar), ubiquity, and gaslike transport properties. In general, CO_2 is a poor solvent for high molecular weight polymers. For example, the solubility pressure of polyisoprene with a molecular weight of 27 kDa exceeds the pressure limitation (2.4 kbar) of a specialized instrument.[10] Amorphous fluoropolymers, such as poly(1,1-dihydroperfluorooctyl acrylate) (PFOA)[11] and perfluorinated polyethers,[12] represent exceptions; they are soluble in CO_2 at pressures less than 200 bar at 25 °C. On this basis, fluoropolymers are a common lyophilic choice for dispersing copolymers in supercritical carbon dioxide ($scCO_2$).[13−17]

Research on the self-assembly of block copolymers in CO_2 has focused on the existence of a critical micelle density (CMD). McClain et al. first reported the formation of polystyrene-*b*-PFOA (PS−PFOA) spherical micelles in $scCO_2$.[18] Using small-angle neutron scattering, Londono et al. further characterized the size of these micelles as a function of solvent density and as a function of copolymer molecular weight, composition, and concentration; spherical micelles were observed at all conditions.[19] Using poly(vinyl acetate)-*b*-poly(1,1,2,2-tetrahydroperfluorooctyl acrylate) (PVAc−PTAN), Buhler et al. established the existence of a reversible aggregate-to-unimer transition in compressible CO_2 as a function of copolymer concentration and solution density.[20] Building on this result, the CMD for PVAc−PFOA was studied extensively using small-angle X-ray scattering,[21,22] small-angle neutron scattering,[23−25] and dynamic light scattering.[22,26−28] Liu et al. performed high-pressure dynamic light scattering measurements (HP−DLS) on solutions of PVAc−PFOA and concluded that despite the notion of a CMD the aggregate-to-unimer transition is not independent of temperature.[22] Small-angle X-ray scattering measurements by Lo Celso et al. substantiated this conclusion; the CMD for PVAc−PFOA in CO_2 decreased slightly with increasing temperature between 30 and 65 °C.[21,23] The kinetic aspects of chain exchange and self-assembly were characterized using small-angle X-ray scattering[29,30] and pulsed field gradient nuclear magnetic spectroscopy.[31] For PS−PFOA, the time scale for chain exchange among micelles was 0.1 s, which is several orders of magnitude less than that for conventional aqueous block copolymer systems.[32]

Aqueous and organic precedents imply the feasibility of nonspherical micelles in selective, compressible solvents. We aim to extend this self-assembly motif to condensed CO_2 using amphiphilic copolymers (LF) of polylactide (PLA) and poly(perfluoropropylene oxide) (PFPO). The glass transition temperature (T_g) of low molecular weight PLA is ca. 40 °C. Implicit in the selection of PLA as the CO_2-phobic, core-forming block is the potential for freezing the LF micelles in CO_2. This technique facilitates direct characterization of the frozen structures by transmission electron microscopy and is analogous to the strategy used by Zhang and Eisenberg[6] to characterize micelles of PS−poly(acrylic acid) in aqueous solutions.

Experimental Section

General Methods. The ^{1}H and ^{19}F NMR spectra were measured using a Varian VAC-300 spectrometer. The PLA samples were prepared in deuterated chloroform, the PFPO samples in 1,1,2-trichlorotrifluoroethane, and the PLA−PFPO copolymer samples in an 80/20 v/v mixed solvent of 1,1,2-trichlorotrifluoroethane and deuterated chloroform. Size exclusion chromatography (SEC) was performed using a Hewlett-Packard 1100 series liquid chromatograph equipped with Jordi polydivinylbenzene columns. The mobile phase was tetrahydrofuran at 40 °C and a flow rate of 1 mL/min.

* Authors for correspondence: lodge@chem.umn.edu, hillmyer@chem.umn.edu.
[†] Department of Chemical Engineering and Materials Science.
[‡] Department of Chemistry.

10.1021/ma0704360 CCC: $37.00
Published on Web 06/13/2007

Materials. All materials were used as received unless otherwise noted. DL-Lactide (Sigma-Aldrich) was recrystallized from ethyl acetate once, dried under vacuum at ambient temperature, and stored under nitrogen. Toluene was purified by passing over a series of two columns: one of activated alumina and the other of supported copper catalyst. Methoxynonafluorobutane (3M, HFE-7100) and α,α,α-trifluorotoluene (Sigma-Aldrich) were stirred over CaH_2 for 12 h and then distilled and stored over activated molecular sieves. Cross-linked polystyrene with pendant 4-aminopyridine (Reilly Industries, polyDMAP) and carboxylic acid end-functionalized PFPO (DuPont, Krytox FS Series) were dried under dynamic vacuum for 12 h at ambient temperature prior to use.

Synthesis of Polylactide-*b*-poly(perfluoropropylene oxide) (LF). The ring-opening polymerization of lactide in toluene was conducted under a nitrogen atmosphere in a Chemglass heavy-walled pressure vessel and sealed using a Viton O-ring and Teflon bushing. In a typical reaction, DL-lactide (12.3 g, 0.085 mol) was dissolved in 90 mL of dry toluene. Addition of 1.28 mL (0.002 mol) of diethylaluminum ethoxide (Sigma-Aldrich, 1.6 M in toluene) initiated the reaction. The solution was stirred at 90 °C for 20 h, and then the polymerization was terminated by adding 5 mL of 1.5 M HCl. The polymer was precipitated in MeOH at 0 °C and dried under dynamic vacuum at 60 °C for 72 h.

To facilitate the coupling of PLA and PFPO, the carboxylic acid end-functionalized PFPO was reacted with oxalyl chloride to form the acid chloride functionality.[33] In a typical reaction, 1−2 g of polyDMAP was added to a single-neck round-bottom flask modified with a Teflon valve sidearm; polyDMAP scavenged the HCl produced by the coupling reaction. PLA (2.5 g, 4.8 kDa, 5.2×10^{-4} mol) was dissolved in 20 mL of α,α,α-trifluorotoluene, and acid chloride end-functionalized PFPO (30 g, 4.2 kDa, 7.1×10^{-3} mol) was dissolved in 50 mL of methoxynonafluorobutane (MnFB). These two solutions were then added to the reaction flask containing polyDMAP under a nitrogen purge; the final molar ratio of PFPO to PLA was ca. 15:1. To achieve homogeneous reaction conditions, both MnFB and α,α,α-trifluorotoluene were added to achieve a final reaction volume of 250 mL; the mixed solvent ratio was 1:1 (v/v). The reaction was refluxed at 65 °C for 24 h, after which the solution was filtered to remove polyDMAP. Excess solvent was removed under reduced pressure, and then the polymer was dried under vacuum at ambient temperature for 12 h. The reaction products were dissolved in tetrahydrofuran at a concentration of 1 wt % and then centrifuged and decanted five times to remove excess PFPO homopolymer. THF was removed under reduced pressure, and the polymer was dried under vacuum at ambient temperature for 72 h.

The following resonances are representative of the homopolymer precursors and the diblock copolymer. PLA ^{1}H NMR (300 MHz, $CDCl_3$): 5.2 (m, −C(O)C**H**(CH_3)O−), 4.4 (m, −C**H**(CH_3)OH), 4.2 (m, CH_3C**H**$_2$O−), 1.6 (m, −C(O)CH(C**H**$_3$)O−). PFPO−COCl ^{19}F (300 MHz, $CF_2ClCFCl_2$): −146 (broad, −C**F**(CF_3)CF_2O−), −131 (broad, CF_3C**F**$_2$$CF_2$O−), −127 (broad, −C**F**(CF_3)C(O)Cl), −82 (broad, −CF(C**F**$_3$)C**F**$_2$O−). PLA−PFPO ^{1}H NMR (300 MHz, $CDCl_3$/$CF_2ClCFCl_2$ 20/80 v/v): The PLA resonances are the same as above with one exception: (PLA−C**H**(CH_3)OC(O)−PFPO) shifts downfield and cannot be distinguished from the peak at 5.2 ppm. ^{19}F NMR (300 MHz, $CDCl_3$/$CF_2ClCFCl_2$ 20/80 v/v): The PFPO resonances are the same as above with one exception: the peak at −127 shifts to −133 ppm (broad, PFPO−C**F**(CF_3)C(O)O−PLA).

Solubility Measurements. The solubility of the block copolymers in CO_2 was determined using a home-built, variable-volume high-pressure cell (see Supporting Information for a schematic of the cell). In a typical cloud point experiment, the polymer sample was loaded directly into the cell, and the cell was purged with CO_2 for 20 min to remove atmospheric gases. The system was charged with CO_2 to 350 bar at ambient temperature, and the contents were stirred using a Teflon-coated stir bar for 30 min to achieve a homogeneous solution. For each temperature measurement, 20 min was allowed for thermal equilibration. After achieving the desired temperature, the cloud point measurements were conducted by increasing the sample volume. The corresponding rate at which the pressure decreased was 5−10 bar/min. The solution cloud point was defined as the pressure at which the stir bar was no longer visible. Each temperature measurement was repeated 3−5 times, and the reported value is the average. The data uncertainties represent the 95% confidence interval determined by 10 replicate measurements at $T = 25$ °C.

Dynamic Light Scattering (DLS). DLS measurements were performed on both conventional liquids and compressible fluids. For conventional measurements, samples were filtered (0.45 μm pore size) into dust-free glass tubes (i.d. of 0.2 in., o.d. of 0.28 in.). For measurements made at ambient temperature with conventional liquids, the DLS tubes were sealed using paraffin film to prevent contamination from dust and water vapor condensation. For measurements performed at elevated temperatures, the tubes were flame-sealed under reduced pressure to prevent solvent evaporation. The DLS setup consisted of a Lexel 75 Ar ion laser with an operating wavelength of 488 nm, a home-built goniometer with a temperature-controlled silicon oil bath, and a Brookhaven Instruments photomultiplier tube (BI-PMT) and digital correlator card (BI-9000AT) for detection and data processing.

Intensity correlation functions $g^{(2)}(\tau)$ were analyzed using two expressions. For systems exhibiting two decay modes, the following double-exponential expression was used

$$g^{(2)}(\tau) - 1 = [A_1 \exp(-\Gamma_1\tau) + A_2 \exp(-\Gamma_2\tau)]^2 \quad (1)$$

where A_1 and A_2 represent the relative contributions to the scattered field of the decay rates, Γ_1 and Γ_2. For systems composed of a single, broad distribution, the following cumulant expansion was used to fit the data[34,35]

$$g^{(2)}(\tau) - 1 = \beta e^{(-2\bar{\Gamma}\tau)}(1 + \mu_2\tau^2/2!)^2 \quad (2)$$

where β is the spatial coherence factor, $\bar{\Gamma}$ is the mean decay rate, and μ_2 is the second cumulant; the ratio of $\mu_2/\bar{\Gamma}^2$ was used as a measure of the mobility dispersity or breadth of the size distribution. Using either eq 1 or 2, Γ was determined for different wave vector values, $q = 4\pi n\lambda^{-1} \sin(\theta/2)$, where n is the solvent refractive index and θ is the scattering angle. The mean diffusion coefficient D_t was determined via a forced fit through zero of Γ vs q^2, and the mean hydrodynamic radius of the micelles was determined using the Stokes−Einstein equation, $D_t = kT/6\pi\eta R_h$. A 95% confidence interval is reported for each of the measured R_h; these uncertainties are based on the standard error associated with the fitted value of D_t. For conventional DLS measurements, where the solvent was methoxynonafluorobutane (MnFB), the refractive index and solvent viscosity η were 1.3 and 0.61 cP. In addition to eqs 1 and 2, the inversion routine CONTIN was used to analyze the intensity correlation functions. CONTIN employs a regularization method to determine the distribution of Γ that satisfies the following the expression[36]

$$g^{(1)}(\tau) = \int_0^\infty G(\Gamma)\, e^{-\Gamma t}\, d\Gamma \quad (3)$$

where $g^{(1)}(\tau)$ is the field correlation function and is related to the intensity correlation function by the Siegert relation, $g^{(2)}(\tau) - 1 = \beta|g^{(1)}(\tau)|^2$.

High-Pressure Dynamic Light Scattering (HP-DLS). The HP-DLS setup used for this study is a modified version of the cell designed by Zhou, Chu, and Dhadwal.[27,28,37] The cell included four optical ports at angles of 0°, 30°, 90°, and 150°. The fifth port at 180° was connected to a safety valve/burst disc assembly (see Figure S4 for a schematic). In addition, this port included a beam stop insert, which was machined from aluminum and anodized black. The upper surface of the sample volume was also anodized black to minimize reflections. The sample (volume 5 mL) was stirred using a Teflon-coated stir bar. The optical ports were composed of GRIN microlenses (NSG America; SLW, 3.0 mm diameter, 7.8 mm long, 0.25 pitch) epoxied onto stainless steel ferrules. For the

incident light source, a Lexel 95 Ar ion laser (operating at a wavelength of 488 nm) was coupled (Newport Corp., F-915) to a multimode fiber (Newport Corp., F-MSD). The scattered light was collected by a single mode fiber (Thorlabs, SMF-28) sheathed with reinforced tubing (Thorlabs, FT900SM) to improve mechanical integrity. The stripped fiber ends were epoxied within ceramic ferrules (SENKO), and the endfaces were polished using 5, 3, and 1 μm polishing paper. The scattered light was detected using a Malvern photomultiplier tube modified with a home-built faceplate. The faceplate contained an optical port identical to those machined into the scattering cell. For each measured angle, the detector probe was inserted into the corresponding optical port. Putty was used to anchor the detector probe and maintain flush contact of the fiber with the rear focal plane of the GRIN microlens. The signal from the discriminator of the PMT was fed to a Brookhaven digital correlator (BI-9000AT). The modifications made from the setup discussed by Zhou et al.[37] were necessary to accommodate the weak scattering; the $dn/dc \approx (n_{PFPO} - n_{CO_2,400\ bar})/\rho_{PFPO}$ of PFPO in CO_2 is $\sim$0.03 mL/g.

To remove dust from the polymer sample, the LF copolymers were dissolved in MnFB, filtered (0.45 μm pore size), and dried under vacuum for 72 h at 40 °C. Prior to each measurement, the cell was thoroughly rinsed with both MnFB and THF and then dried at 50 °C. As a final cleaning step, the sample volume was flushed with CO_2 for 1 h and then fluidized with CO_2 at a pressure of 400 bar and stirred for 1 h. At ambient pressure, the filtered and dried polymer sample was loaded into the cell through the fifth port at 180°; typically, 40 mg was added to achieve the desired concentration of 1 wt % in solution. To purge air and dust, the cell was flushed with CO_2 and then pressurized to the desired solvent density. After stirring the solution for 12 h, the intensity correlation functions were measured. For the data analysis, the refractive index and viscosity values for CO_2 were taken from Burns et al.[38] and Fenghour et al.,[39] respectively. At 400 bar and 25 °C, these are 1.245 and 0.13 cP. The DLS measurements were limited to delay times longer than 10^{-6} s to avoid artifacts due to afterpulsing.

Quenched Micelle Solution Preparation. To characterize the micelles using conventional microscopy techniques, solutions of an LF copolymer in CO_2 were cooled at constant solvent pressure, quenched, and dispersed again in an analogous F selective solvent. In a typical experiment, the block copolymer was dissolved in CO_2 at a pressure of 350 bar and ambient temperature. The clear, homogeneous solution was stirred for 96 h and then cooled to −1 °C at constant pressure using a recirculating water/ethylene glycol solution; the cooling process took place over the course of 8 h. We performed HP-DLS measurements on the micellar solution at 25 °C and at a cooled temperature of 5 ± 2 °C to verify that there was no structural evolution associated with the cooling process (see Supporting Information). After cooling the system, CO_2 was released from the cell rapidly; this expansion acted to further cool the system. We did not attempt to decouple the two cooling processes to determine which was the more critical in quenching the micelle structures. After venting CO_2, cold MnFB was added to the cell, and the solution was stirred for 48 h to resolvate the frozen aggregates. The recovered MnFB solution was filtered (0.45 μm pore size) to remove dust and residual material that did not fully redisperse.

Trasmission Electron Microscopy (TEM). TEM samples were prepared on carbon-coated copper grids (Ted Pella, No. 01753-F) using two strategies. The first involved depositing a drop of solution onto a grid and blotting excess solvent. These grids were imaged under vacuum at ambient temperature using a JEOL 1210 microscope operating at 120 keV. When the grids were prepared in this manner, the observed structures were often clusters of micelles. Consequently, we devised a second strategy where the grids were prepared using a controlled vitrification environment system (CEVS). After depositing a drop of solution on the grid and blotting the excess, the grid was plunged into liquid nitrogen, and the cast film was vitrified. For imaging, the samples were transferred to a cryogenic sample stage (Gatan 626) and were maintained at −178 °C. Micrographs were captured with a Gatan 724 multiscan CCD camera; the optical density gradients of the background were digitally subtracted. Typically, this "cyro-casting" technique produced grids coated with a thin solvent film. Block copolymer micelles were embedded in the vitrified film, and no clusters were observed.

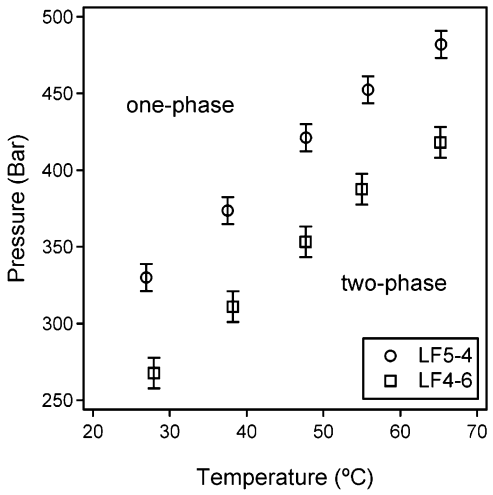

Figure 1. Cloud point pressure as a function of temperature for LF copolymers in condensed CO_2 at a concentration of 1 wt %. The error bars represent the 95% confidence interval determined by 10 replicate measurements at 25 °C.

Results and Discussion

For this study, two diblock copolymers were synthesized, LF5-4 and LF4-6, where the numerals reflect the constituent polymer molecular weights in kDa (see Supporting Information for SEC and ^{1}H NMR analysis). The PFPO volume fraction of these diblock copolymers was 0.49 for LF4-6 and 0.37 for LF5-4. Both blocks were of comparable total molecular weight. To form cylindrical micelles or vesicles in solution, the copolymer volume fraction of the CO_2-philic PFPO was designed to be substantially lower than that of copolymers previously studied in CO_2.[18]

LF copolymer solubility at 1 wt % in liquid and supercritical CO_2 was measured as a function of temperature (Figure 1). The data represent lower critical solution temperatures; upon heating at a fixed pressure, phase separation occurs. LF4-6 is soluble at lower pressures than LF5-4, a result that is consistent with the higher PFPO volume fraction. The solubility of the LF copolymers is less than that reported for the highly asymmetric copolymer PVAc−PFOA(10−60 kDa), which is soluble at 200 bar and 45 °C.[20] This is likely a consequence of the lower lyophilic volume fraction (0.5 for LF4-6 vs 0.8 for PVAc−PFOA) and the enhanced CO_2 solubility of the constituent blocks, PVAc and PFOA, relative to their LF counterparts.[11,40,41] However, the LF copolymers are more soluble than copolymers of PS−poly(perfluorooctylethylenoxymethylstyrene) (PFDS) (8−21 kDa), which are insoluble at a pressure of 380 bar and a concentration of 4 wt %.[42] Given the stark CO_2 solubility difference between PLA[43] and PFPO,[12] the LF copolymers are amphiphilic and expected to form micelles in solution; this hypothesis was tested using HP-DLS.

HP-DLS experiments were performed on the LF copolymers at 1 wt % and a single pressure and temperature, 400 bar and 25 °C, where the system was well into the "one-phase" region for both copolymers. Figure 2A is the measured intensity correlation function at $\theta = 30°$ for LF4-6. The data collected at 30° and 90° were fit using a double-exponential, eq 1, to determine the decay rate Γ for each diffusive mode.[44] The inset figure plots Γ vs the wave vector squared; the corresponding

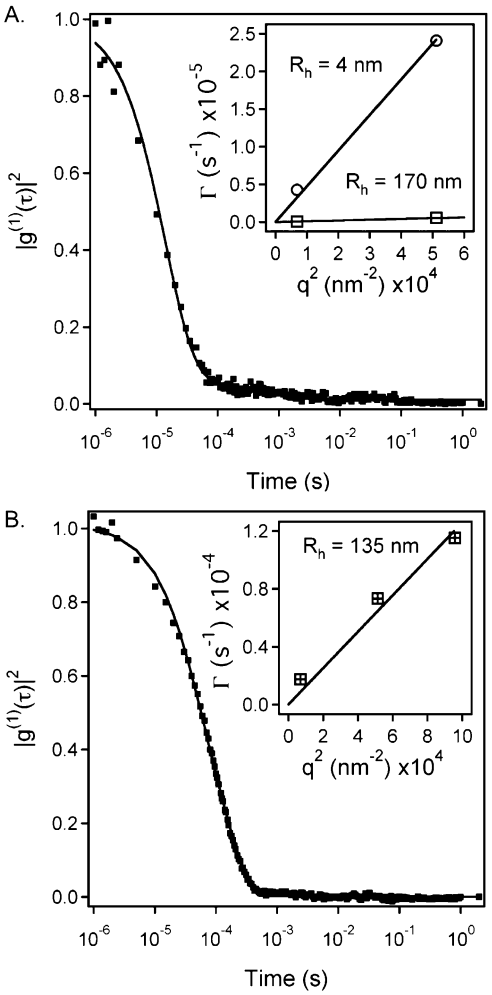

Figure 2. Intensity correlation functions for (A) LF4-6 at $\theta = 30°$ and (B) LF5-4 at $\theta = 90°$ in condensed CO_2 at 25 °C and 400 bar. The figure insets represent the size of the micelles determined by fitting the decay rate vs wave vector squared.

mean R_h values for each diffusive mode were 4 ± 2 and 170 ± 35 nm. The normalized intensity-weighted amplitudes of the two modes were 0.2 (170 nm) and 0.8 (4 nm); therefore, the 4 nm particles represent ~99% of the total particles by number. Given the amphiphilic nature of LF4-6 and the measured size, the 4 nm aggregates are most likely spherical micelles (vide infra). This result is consistent with previously reported dimensions for spherical micelles of PVAc−PFOA, where for a 53 kDa copolymer the spherical micelles had a mean R_h of 20 nm.[28] Explicit determination of aggregate structure will be considered further for the case of LF5-4 in CO_2.

Figure 2B is a plot of the DLS results for LF5-4. The intensity correlation functions at 30°, 90°, and 150° were fit using the cumulant expansion, eq 2.[45] The inset figure is a plot of $\bar{\Gamma}$ vs q^2 to determine D_t for the structures. In eq 2, the second cumulant μ_2 accounts for a distribution of particle sizes about the mean value, and the mobility dispersity $\mu_2/\bar{\Gamma}^2$ is a measure of the breadth of the distribution. For spherical micelles, the typical value of $\mu_2/\bar{\Gamma}^2$ is less than 0.1, which is characteristic of a narrow size distribution. For LF5-4 in CO_2, the mobility dispersity at $\theta = 90°$ was 0.5 and is indicative of a broad or multimodal size distribution.

In addition, the DLS results indicate a mean R_h of 135 ± 40 nm for the block copolymer aggregates. Given that the fully stretched chain length of LF5-4 is estimated to be 30 nm, the observed structures are too large to be spherical micelles. This hypothesis was explored using a quenching strategy to freeze the micelles in CO_2 and then characterize them using conventional TEM techniques (see Experimental Section). Since this technique is unprecedented for block copolymers dispersed in a compressible solvent, we will present results for two control experiments.

The essence of the first control experiment was to contrast the DLS results for kinetically frozen LF5-4 micelles redispersed in MnFB against those for a solution of "pristine" micelles. This pristine solution of LF5-4 was prepared by directly dissolving the copolymer in MnFB, stirring at 65 °C for 72 h, and cooling the solution to ambient temperature. Figure 3A presents the normalized intensity correlation function at $\theta = 90°$ for the LF5-4 micelles quenched in CO_2 and redispersed in MnFB, the LF5-4 micelles measured in CO_2, and the pristine solution. (Note the measurements are performed in two different solvents; thus, the time axis of the measured correlation function has been shifted to account for the difference in solvent viscosity between CO_2 and MnFB.) Figure 3A indicates the quenched and in situ solutions are in good agreement and in sharp contrast to the pristine solution.

Figure 3B is a plot of the mean decay rate determined using eq 1 as a function of wave vector for each of the three data sets. From the Stokes−Einstein equation, the mean R_h for the pristine micelles was 13 ± 1 nm, 70 ± 3 nm for the quenched, and 135 ± 40 nm for those measured in situ. Superficially, these results indicate the quenched micelles are consistent with those characterized in situ. However, there is a quantitative difference in the measured R_h value for the two cases. This difference is plausible given the unlikelihood of completely redispersing the quenched micelles. In fact, one might expect the larger particles in solution to coagulate on venting CO_2, thereby skewing the DLS results for the quenched data set to a smaller size. The cumulant analysis of the correlation functions yields insight into the breadth of the aggregate sizes in solution. The mobility dispersity $\mu_2/\bar{\Gamma}^2$ for the pristine micelles determined at $\theta = 90°$ was 0.08. As for the measured sizes, this result is in contrast to and much smaller than that for the quenched micelles (0.3) and those measured in CO_2 (0.5).

To further compare the three samples, CONTIN distributions determined using the autocorrelation data at $\theta = 90°$ are shown in Figure 3C. In this plot, the line width amplitude is given as $\Gamma G(\Gamma)$ to more accurately reflect the number-weighted size distribution in solution. The agreement of the CONTIN results for the quenched and in situ solutions is stronger than that of the cumulant analysis. The inversion method indicates both samples are bimodal with particle sizes of 100 and 5−10 nm. The slight discrepancy in the peak location for the small size distribution is a consequence of the uncertainty introduced by measuring the intensity correlation function in a compressible solvent, where the viscosity is 0.13 cP. This gaslike viscosity shifts the characteristic time scale for fast decay rates to delay times outside the measurable range. Consequently, the measured intensity correlation function is incomplete, and an inversion routine may not give unique results.[46] Overall, Figure 3 strongly suggests the quenched and in situ aggregate structures are physically similar.

For the second control experiment, the kinetically frozen micelles of LF5-4 redispersed in MnFB were heated to determine whether the aggregate structures recovered their "pristine" state. The solutions were heated at 70 °C for an extended period of time, and the intensity correlation function of the solution was monitored. Data were collected at a single angle $\theta = 90°$, and the intensity correlation functions were fit

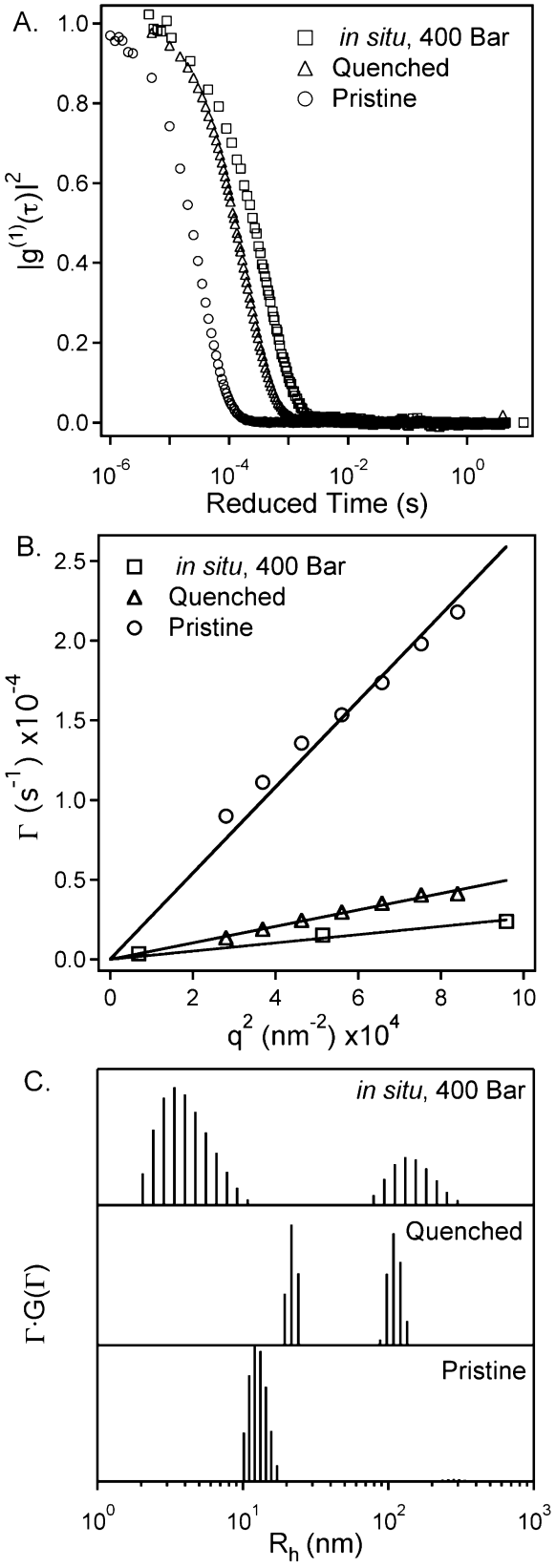

Figure 3. Comparison of DLS data for pristine, quenched, and in situ LF5-4 samples. Plots of (A) the intensity correlation function at $\theta = 90°$, (B) the mean decay rate (cumulant), and (C) the distribution of R_h (CONTIN) are included for each solution. Note the time axis and Γ values in (A) and (B) have been normalized to account for the difference in viscosity between CO_2 and MnFB.

using the cumulant analysis, eq 2. Figure 4 is a plot of the cumulant fits as a function of annealing time. Autocorrelation functions for both the initial quenched and pristine micelle solutions are included as reference points. With annealing time, the measured decay rate increases, and the autocorrelation function approaches that of the pristine case. The full recovery of the pristine result was not experimentally tractable due to a decrease in the scattered intensity of the solution; the disappearance of the large structures led to an order of magnitude decrease in measured intensity. In addition, the concentration of the quenched solution was ca. 5 times lower than that of the pristine micelle solution (1 wt %).

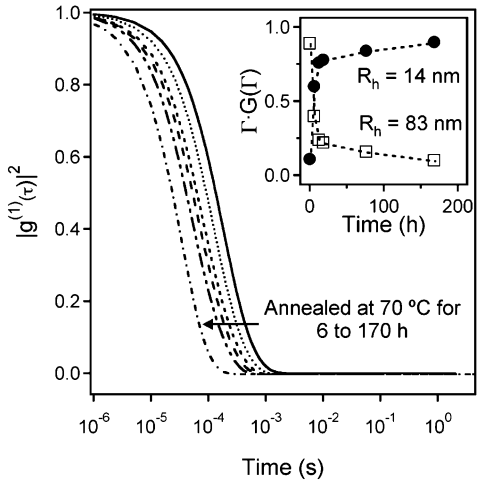

Figure 4. Cumulant curve fits of the intensity correlation function for pristine (-•-) and quenched (—) LF5-4 micelles in MnFB and the quenched micelles annealed at 70 °C for 0−170 h. The inset indicates the recovery of the pristine micelle size on heating.

To further analyze the evolution of the sample, the autocorrelation function data were fit using a global, double-exponential expression (eq 1). The global fitting parameters were Γ_1 and Γ_2, and the data set specific variables were the intensity-weighted amplitudes A_1 and A_2. For the pristine sample, A_1 was set to zero, reducing eq 1 to a single-exponential fit. From the global fit, the hydrodynamic radii of the micelles were 14 and 83 nm, which is consistent with the results plotted in Figure 3C. As the quenched solution was heated at 70 °C, the absolute scattered intensity decreased, coincident with the reorganization of the 83 nm micelles to purely spherical micelles of $R_h = 14$ nm. Using the fit values of A_1 and A_2, the normalized number distributions of the two species in solution were approximated as $\Gamma_i A_i/(\Gamma_i A_i + \Gamma_j A_j)$. The inset of Figure 4 illustrates how the distribution of sizes changed with annealing time. This annealing of the solution at a temperature above the glass transition of PLA ($T_g \sim 40$ °C) facilitated unimer exchange and, subsequently, the frozen micelles equilibrated. In fact, the LF5-4 chains recover their pristine state of spherical micelles within the first 24 h of heating.

The DLS results demonstrated that LF5-4 micelles were successfully quenched in liquid CO_2. This technique facilitates direct characterization of the structures via TEM. The images are shown in Figure 5. Images A and B correspond to samples that were prepared by vitrifying the sample and maintaining it at −178 °C throughout the imaging process. Image C corresponds to a sample that was maintained at ambient conditions. The key difference among the samples is the presence of vitrified solvent in image B of Figure 5. The electron density of MnFB is 0.72 mol e^-/cm^3 and is higher than the density of PLA, which is 0.66 mol e^-/cm^3. As a result, the structures in image B exhibit "reverse" contrast; the PLA core of the micelle appears lighter than the solvent matrix. Despite a similar preparation protocol, this is not readily apparent in image A. This is most likely the

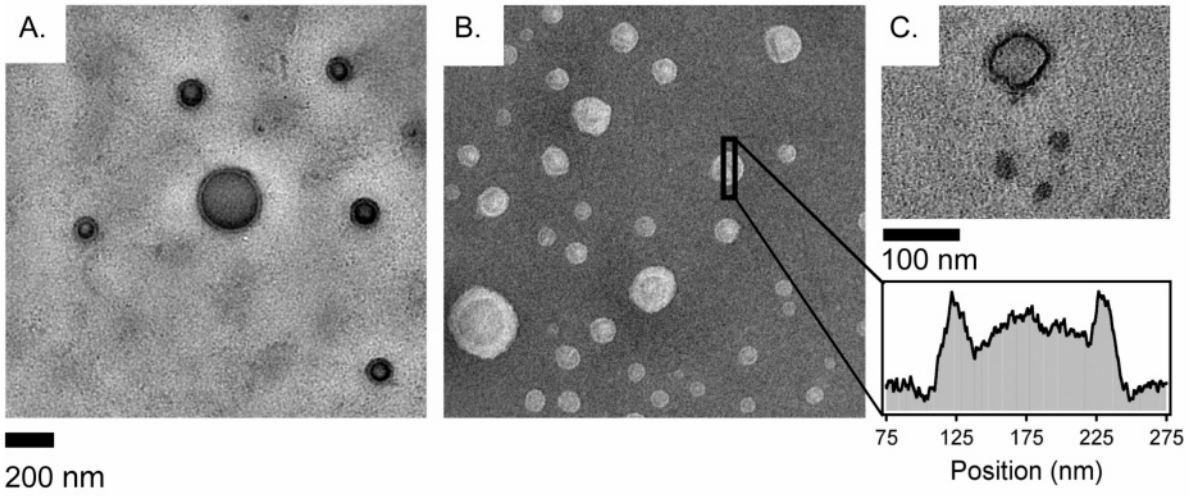

Figure 5. Transmission electron micrographs of frozen LF5-4 vesicles quenched in liquid CO_2 and cast from MnFB. Images A and B are for grid samples that were vitrified and maintained at −178 °C. Image C is for a sample prepared and maintained under ambient conditions. Finally, an intensity profile is included for the selected micelle in image B.

consequence of solvent evaporation prior to vitrification. The aggregate structures in the micrographs are circular with radii ranging from 50 to 150 nm, which is consistent with the DLS results reported in Figure 3C. A profile of the transmitted electron intensity for a selected micelle is also included in Figure 5. Characteristic of vesicles, the profiled structure exhibits two intensity peaks that are coincident with the concentric PLA shell. Nearly all of the vesicles imaged in Figure 5 exhibit a PLA shell thickness of 15 nm. There are a few exceptions in image B, where the structures may be partially collapsed or sublimation of the solvent has left a void surrounding the micelles. In addition to vesicles, we did observe the formation of large, compound micelles (see Figure S7). These structures are most likely an artifact of the quenching process.

The micrograph in Figure 5C indicates the coexistence of spherical micelles with vesicles for the quenched LF5-4 solution. The core radius of these observed spherical micelles is ca. 5−6 nm. In Figure 3C, the inversion of the DLS data for LF5-4 indicated the formation of similarly sized structures with R_h values from 2 to 10 nm; thereby, these results are quantitatively consistent. For the LF4-6 DLS results, we asserted that the measured structures with a mean R_h of 4 ± 2 nm were spherical micelles. The higher PFPO volume fraction of LF4-6 relative to LF5-4 dictates structures with lower aggregation numbers and, hence, smaller sizes than the spherical micelles imaged in Figure 5C.[47] Thus, the measured LF4-6 structures are most likely spherical micelles. However without micrograph evidence for LF4-6, we cannot rule out the possibility that the chains exist as single-chain unimers in solution, especially given the estimated fully stretched chain length of 30 nm.

Conclusions

The copolymer system of PLA−PFPO is a model system for studying the effects of copolymer volume fraction on micelle morphology in solution. Copolymers with an overall molecular weight of 10 kDa are soluble at CO_2 densities greater than 0.97 g/mL. Using a combination of dynamic light scattering and transmission electron microscopy, we demonstrated the formation of block copolymer vesicles in liquid CO_2. This result partially extends the classic micelle morphology motif from conventional aqueous and organic solvents to potential solvent alternatives, such as condensed CO_2.

Acknowledgment. This work was supported in part by the MRSEC Program of the National Science Foundation under Award DMR-0212302. W. F. Edmonds thanks 3M for their support through the 3M Graduate Science and Technology Fellowship and the University of Minnesota Graduate School for their support through the Doctoral Dissertation Fellowship. The authors thank Dr. Benjamin Chu (SUNY at Stony Brook) for graciously lending us his high-pressure dynamic light scattering cell.

Supporting Information Available: Schematics of the cloud point and high-pressure dynamic light scattering instruments, NMR and SEC characterization of the LF block copolymers, HP-DLS results for the LF5-4 solution at 350 bar (25 °C), 400 bar (25 °C), and 400 bar (5 °C), and a micrograph of the artifacts observed as a consequence of quenching. This material is available free of charge via the Internet at http://pubs.acs.org.

References and Notes

(1) Zupancich, J. A.; Bates, F. S.; Hillmyer, M. A. *Macromolecules* **2006**, *39*, 4286.
(2) Jain, S.; Bates, F. S. *Science* **2003**, *300*, 460.
(3) Shen, H.; Eisenberg, A. *Macromolecules* **2000**, *33*, 2561.
(4) Bang, J.; Jain, S.; Li, Z.; Lodge, T. P.; Pedersen, J. S.; Kesselman, E.; Talmon, Y. *Macromolecules* **2006**, *39*, 1199.
(5) Shen, H.; Eisenberg, A. *J. Phys. Chem. B* **1999**, *103*, 9473.
(6) Zhang, L.; Eisenberg, A. *Science* **1995**, *268*, 1728.
(7) LaRue, I.; Adam, M.; Pitsikalis, M.; Hadjichristidis, N.; Rubinstein, M.; Sheiko, S. S. *Macromolecules* **2006**, *39*, 309.
(8) Ding, J.; Liu, G.; Yang, M. *Polymer* **1997**, *38*, 5497.
(9) Riess, G. *Prog. Polym. Sci.* **2003**, *28*, 1107.
(10) McHugh, M. A.; Park, I.-H.; Reisinger, J. J.; Ren, Y.; Lodge, T. P.; Hillmyer, M. A. *Macromolecules* **2002**, *35*, 4653.
(11) Hsiao, Y.-L.; Maury, E. E.; DeSimone, J. M.; Mawson, S.; Johnston, K. P. *Macromolecules* **1995**, *28*, 8159.
(12) Hoefling, T. A.; Enick, R. M.; Beckman, E. J. *J. Phys. Chem.* **1991**, *95*, 7127.
(13) Hwang, H. S.; Kim, H. J.; Jeong, Y. T.; Gal, Y.-S.; Lim, K. T. *Macromolecules* **2004**, *37*, 9821.
(14) Lim, K. T.; Kim, H. J.; Jin, S.-H.; Choi, S.-J.; Gal, Y. S. *Stud. Surf. Sci. Catal.* **2004**, *153*, 251.
(15) Hwang, H. S.; Heo, J. Y.; Jeong, Y. T.; Jin, S.-H.; Cho, D.; Chang, T.; Lim, K. T. *Polymer* **2003**, *44*, 5153.
(16) Lim, K. T.; Lee, M. Y.; Moon, M. J.; Lee, G. D.; Hong, S.-S.; Dickson, J. L.; Johnston, K. P. *Polymer* **2002**, *43*, 7043.
(17) Ye, W.; Wells, S.; DeSimone, J. M. *J. Polym. Sci., Part A: Polym. Chem.* **2001**, *39*, 3841.

(18) McClain, J. B.; Betts, D. E.; Canelas, D. A.; Samulski, E. T.; DeSimone, J. M.; Londono, J. D.; Cochran, H. D.; Wignall, G. D.; Chillura-Martino, D.; Triolo, R. *Science* **1996**, *274*, 2049.
(19) Londono, J. D.; Dharmapurikar, R.; Cochran, H. D.; Wignall, G. D.; McClain, J. B.; Betts, D. E.; Canelas, D. A.; DeSimone, J. M.; Samulski, E. T.; Chillura-Martino, D.; Triolo, R. *J. Appl. Crystallogr.* **1997**, *30*, 690.
(20) Buhler, E.; Dobrynin, A. V.; DeSimone, J. M.; Rubinstein, M. *Macromolecules* **1998**, *31*, 7347.
(21) Lo Celso, F.; Triolo, A.; Triolo, F.; Donato, D. I.; Steinhart, M.; Kriechbaum, M.; Amenitsch, H.; Triolo, R. *Eur. Phys. J. E* **2002**, *8*, 311.
(22) Liu, L.-Z.; Cheng, Z.; Inomata, K.; Zhou, S.; Chu, B. *Macromolecules* **1999**, *32*, 5836.
(23) Lo Celso, F.; Triolo, A.; Triolo, F.; McClain, J. B.; DeSimone, J. M.; Heenan, R. K.; Amenitsch, H.; Triolo, R. *Appl. Phys. A: Mater. Sci. Process.* **2002**, *74*, S1427.
(24) Triolo, R.; Triolo, A.; Triolo, F.; Steytler, D. C.; Lewis, C. A.; Heenan, R. K.; Wignall, G. D.; DeSimone, J. M. *Phys. Rev. E* **2000**, *61*, 4640.
(25) Triolo, F.; Triolo, A.; Triolo, R.; Londono, J. D.; Wignall, G. D.; McClain, J. B.; Betts, D. E.; Wells, S.; Samulski, E. T.; DeSimone, J. M. *Langmuir* **2000**, *16*, 416.
(26) Koga, T.; Zhou, S.; Chu, B. *Appl. Opt.* **2001**, *40*, 4170.
(27) Zhou, S.; Chu, B. *Macromolecules* **1998**, *31*, 5300.
(28) Zhou, S.; Chu, B. *Macromolecules* **1998**, *31*, 7746.
(29) Triolo, A.; Lo Celso, F.; Triolo, F.; Amenitsch, H.; Steinhart, M.; Thiyagarajan, P.; Wells, S.; DeSimone, J. M.; Triolo, R. *J. Non-Cryst. Solids* **2002**, *307*, 725.
(30) Lo Celso, F.; Triolo, A.; Triolo, F.; Thiyagarajan, P.; Amenitsch, H.; Steinhart, M.; Kriechbaum, M.; DeSimone, J. M.; Triolo, R. *J. Appl. Crystallogr.* **2003**, *36*, 660.
(31) Cain, J. B.; Zhang, K.; Betts, D. E.; DeSimone, J. M.; Johnson, C. S., Jr. *J. Am. Chem. Soc.* **1998**, *120*, 9390.
(32) Creutz, S.; van Stam, J.; Antoun, S.; De Schryver, F. C.; Jérôme, R. *Macromolecules* **1997**, *30*, 4078.
(33) Li, Z.; Hillmyer, M. A.; Lodge, T. P. *Macromolecules* **2004**, *37*, 8933.
(34) Koppel, D. E. *J. Chem. Phys.* **1972**, *57*, 4814.
(35) Frisken, B. J. *Appl. Opt.* **2001**, *40*, 4087.
(36) Provencher, S. W. *Comput. Phys. Commun.* **1982**, *27*, 229.
(37) Zhou, S.; Chu, B.; Dhadwal, H. S. *Rev. Sci. Instrum.* **1998**, *69*, 1955.
(38) Burns, R. C.; Graham, C.; Weller, A. R. M. *Mol. Phys.* **1986**, *59*, 41.
(39) Fenghour, A.; Wakeham, W. A.; Vesovic, V. *J. Phys. Chem. Ref. Data* **1998**, *27*, 31.
(40) Shen, Z.; McHugh, M. A.; Xu, J.; Belardi, J.; Kilic, S.; Mesiano, A.; Bane, S.; Karnikas, C.; Beckman, E.; Enick, R. *Polymer* **2003**, *44*, 1491.
(41) Chillura-Martino, D.; Triolo, R.; McClain, J. B.; Combes, J. R.; Betts, D. E.; Canelas, D. A.; DeSimone, J. M.; Samulski, E. T.; Cochran, H. D.; Londono, J. D.; Wignall, G. D. *J. Mol. Struct.* **1996**, *383*, 3.
(42) Lacroix-Desmazes, P.; André, P.; DeSimone, J. M.; Ruzette, A.-V.; Boutevin, B. *J. Polym. Sci., Part A: Polym. Chem.* **2004**, *42*, 3537.
(43) Conway, S. E.; Byun, H. S.; McHugh, M. A.; Wang, J. D.; Mandel, F. S. *J. Appl. Polym. Sci.* **2001**, *80*, 1155.
(44) As a consequence of the small structure size (4 nm) and viscosity of CO_2 at these conditions (0.13 cP), the apparent decay rate at 150° was shifted to delay times outside the measurable range.
(45) Equation 2 was used to fit the data in Figure 2B because the double-exponential fit does not capture both modes at $\theta = 150°$. The contribution to the correlation function of the particles at 5 nm (see Figure 3C) is most likely too small to measure at this angle.
(46) Štěpánek, P. In *Dynamic Light Scattering: The Method and Some Applications*; Brown, W., Ed.; Clarendon Press: Oxford, 1993; p 177.
(47) Zhulina, E. B.; Adam, M.; LaRue, I.; Sheiko, S. S.; Rubinstein, M. *Macromolecules* **2005**, *38*, 5330.

MA0704360